



Published in final edited form as:

Biochim Biophys Acta. 2016 April ; 1858(4): 725–732. doi:10.1016/j.bbamem.2016.01.003.

Single-cell, Time-resolved Study of the Effects of the Antimicrobial Peptide Alamethicin on *Bacillus subtilis*

Kenneth J. Barns^a and James C. Weisshaar^{a,b,*}

^aDepartment of Chemistry, University of Wisconsin-Madison, 1101 University Avenue, Madison, WI 53706 USA

^bMolecular Biophysics Program, University of Wisconsin-Madison, 1101 University Avenue, Madison, WI 53706 USA

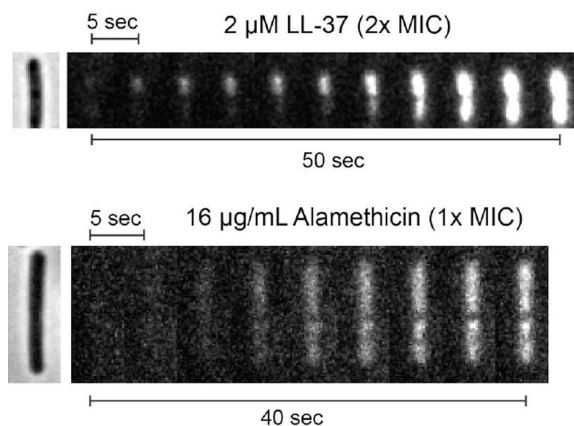
Abstract

Alamethicin is a well studied antimicrobial peptide (AMP) that kills Gram positive bacteria. It forms narrow, barrel stave pores in planar lipid bilayers. We present a detailed, time-resolved microscopy study of the sequence of events during the attack of alamethicin on individual, live *Bacillus subtilis* cells expressing GFP in the cytoplasm. At the minimum inhibitory concentration (MIC), the first observed symptom is the halting of growth, as judged by the plateau in measured cell length vs time. The data strongly suggest that this growth-halting event occurs prior to membrane permeabilization. Gradual degradation of the proton motive force, inferred from a decrease in pH-dependent GFP fluorescence intensity, evidently begins minutes later and continues over about 5 min. There follows abrupt permeabilization of the cytoplasmic membrane to the DNA stain Sytox Orange and concomitant loss of small osmolytes, causing observable cell shrinkage presumably due to decreased turgor pressure. This permeabilization of the cytoplasmic membrane occurs uniformly across the entire membrane, not locally, on a timescale of 5 s or less. GFP gradually leaks out of the cell envelope, evidently impeded by the shrunken peptidoglycan layer. Disruption of the cell envelope by alamethicin occurs in stages, with larger and larger species permeating the envelope as time evolves over tens of minutes. Some of the observed symptoms are consistent with formation of barrel stave pores, but the data do not rule out “chaotic pore” or “carpet” mechanisms. We contrast the effects of alamethicin and the human cathelicidin LL-37 on *B. subtilis*.

Graphical abstract

*Corresponding author: weisshaar@chem.wisc.edu; 608-262-0266.

Publisher's Disclaimer: This is a PDF file of an unedited manuscript that has been accepted for publication. As a service to our customers we are providing this early version of the manuscript. The manuscript will undergo copyediting, typesetting, and review of the resulting proof before it is published in its final citable form. Please note that during the production process errors may be discovered which could affect the content, and all legal disclaimers that apply to the journal pertain.



Time-dependent images from fluorescence microscopy compare the staining of the *B. subtilis* chromosomal DNA by Sytox Orange after treatment with the antimicrobial peptides LL-37 and alamethicin. Cytoplasmic permeabilization is localized for LL-37, but delocalized for alamethicin.

Keywords

Antimicrobial peptide; alamethicin; real-time imaging; single-cell imaging; fluorescence microscopy; *Bacillus subtilis*; membrane permeabilization; barrel stave pore

1. Introduction

Alamethicin is a natural antimicrobial peptide (AMP) produced by fungi of the genus *Trichoderma*. It was discovered in the late 1960's and has been studied as a model pore-forming peptide for decades [1, 2]. Alamethicin has an unusual primary sequence that includes non-standard amino acids and C- and N-terminal modifications. In contrast to the commonplace highly cationic AMPs, the 20-residue isoform F50 bears no charges on either the termini or the sidechains. The peptide exhibits antimicrobial activity against Gram-positive bacteria, but not Gram-negative bacteria [1, 2].

When bound to lipid bilayers, alamethicin forms amphipathic helices with polar residues aligning on one helical face [3]. Neutron and x-ray scattering studies show that alamethicin can form barrel-stave pores in model lipid multilayers composed of phosphatidylcholine [4, 5]. In contrast to the more common toroidal pores, such barrel-stave pores are lined with amphipathic helices entirely oriented perpendicular to the bilayer plane, with the lipids maintaining their normal orientation. This likens the peptide to a “channel-former”, which is consistent with conductance data taken on planar lipid bilayers exposed to alamethicin [6]. At low peptide/lipid (P/L) ratios, the conductance of such pores varies, presumably due to fluctuation of the number of alamethicin monomers engaged in the pore. At higher P/L ratio, neutron scattering from multilayers shows that alamethicin forms stable, closely packed lattices of pores whose inside diameter (~1.8 or 2.6 nm) depends on the lipid used [4]. For the mycoplasma *Spiroplasma melliferum*, treatment with alamethicin leads to dissipation of the proton-motive force (pmf) followed by lysis, suggesting that the formation of small pores may not fully describe the antimicrobial action [7].

The primary sequence for the F50 isoform of alamethicin is [8]: AcU-P-U*-A*-U*-A*-Q-U-V*-U-G-L*-U-P-V*-U-U*-Q-Q-Fol. Here U is α -methylalanine, AcU is acetylated α -methylalanine, and Fol is phenylalaninol. An asterisk next to an amino acid indicates heterogeneity in the actual residue at that location. For example, alamethicin F50 has glutamine (Q) at position 18, while alamethicin F30 has glutamic acid (E). The alamethicin sequence depends on the growth conditions for the fungus [8].

We have been developing single-cell, real-time fluorescence assays aimed at providing a detailed, time-resolved picture of the sequence of events following treatment of live bacterial cells with antimicrobial peptides [9–13]. One goal of this work is to discover the degree to which the well studied translocation and pore-forming properties of AMPs as they interact with model lipid bilayers [14] are relevant to growth-halting mechanisms during attack on live bacteria, whose membranes are far more complex. Here we present a detailed study of the effects of alamethicin on *B. subtilis* cells. Measurement of cell length vs time indicate that cell growth halts several minutes before the proton-motive force (pmf) dissipates. Still later, we observe a sequence of events showing gradual permeabilization of the *B. subtilis* cell envelope to larger and larger species as time goes on. The initial growth halting mechanism is evidently not membrane permeabilization. Imaginable mechanisms include disruption of cell wall synthesis and induction of oxidative stress.

2. Materials and Methods

2.1. Chemicals

All experiments used ultrapure water ($>18\text{ M}\Omega$) from a Millipore Simplicity 185 filter system. Alamethicin was purchased from Sigma-Aldrich ($>98\%$, Catalog no. A4665) and dissolved in ethanol to make a 5 mg/mL stock solution. Sigma-Aldrich states only that the sample is predominantly the F50 form, with trace amounts of the F30 form. LL-37 was purchased from Anaspec (95% pure, Catalog no. 61302, Fremont, CA) and dissolved in water to make a 1 mM stock solution. The DNA stain Sytox Orange (Molecular Probes, Catalog no. S11368) was obtained as a 5 mM solution in DMSO. A 5 μM working solution of Sytox Orange was made in water. The sodium salt of the ionophore nigericin (Sigma Aldrich, Catalog no. N7143, 98% pure) was dissolved in ethanol. Chicken egg-white lysozyme (Sigma-Aldrich, Catalog no. L4919, Bioultra, 98% pure) was dissolved in water. Supplements used for the chemically defined growth medium (5X EZ supplement Beta, M3104; 10X ACGU Beta, M3103; 10X MOPS mix, M2137) were purchased from Teknova.

2.2. Strains and Growth Conditions

B. subtilis 168 from the Bacillus Genetic Stock Center (BGSC, code 1A1) was the parent strain. Most experiments used a strain transformed with plasmid pAD43-25, which expresses cytoplasmic GFP for fluorescence imaging, as described previously [11]. The GFP variety is GFPmut3, whose fluorescence yield is dependent on pH [15, 16]. The GFP strain was grown with 5 $\mu\text{g}/\text{mL}$ chloroamphenicol to select for the plasmid. Chloroamphenicol was omitted when imaging the strain. Strains were grown in *subtilis*-EZ rich, defined medium (here “s-EZRDM”) [11] at 37 °C and 200 rpm (0.9 g) in a New Brunswick Excella E24 Incubator-Shaker. Cultures were grown overnight, inoculated from frozen glycerol stock.

The following day, dilutions of at least 1/200 were made into pre-warmed *s*-EZRDM. Cells were grown to an OD of 0.04–0.06 (600 nm, 1 mm path length) as measured by a Nanodrop 2000 spectrometer from Thermo Scientific, then harvested for microscopy or MIC measurements. The doubling time for both strains in *s*-EZRDM in these conditions is 20 min.

2.3. Minimum Inhibitory Concentration (MIC) Assay

The MIC was measured only for wild type *B. subtilis*. A serial dilution of alamethicin was performed in one row of a polystyrene 96-well plate in *s*-EZRDM, beginning at 128 µg/mL and with twofold dilution at each step. The final volume in each well in the row was 50 µL after serial dilution. A liquid cell culture was grown in the same conditions as described above to a final OD of 0.04–0.06 (1 mm path). This culture was diluted in *s*-EZRDM to an OD of 0.005. 50 µL of the diluted culture was added to each well of the alamethicin serial dilution, so that the maximum concentration tested was 64 µg/mL. The initial OD in each well was 0.0025, and the volume was 100 µL. A second row contained 50 µL of *s*-EZRDM plus 50 µL of inoculum (positive growth control), while a third row contained 100 µL of *s*-EZRDM in each well (negative growth control and blank for OD measurements). The plate was incubated at 37 °C while shaking at 200 rpm (0.9 g) in an Excella 24 Incubator/Shaker from New Brunswick Scientific for 6 hr. This “6-hr MIC” is reported as the lowest concentration for which no cell growth could be detected after 6 hr, as determined by measurements of OD at 595 nm using a Wallac EnVision 2100 Multilabel Reader from Perkin–Elmer. The MIC experiments were performed three times, and were reproducible to within a dilution factor of two. The 6-hr MIC for alamethicin was 16 µg/mL. We cannot report an exact molar concentration, since our sample is a mixture of different isoforms. Assuming an approximate molecular weight of 2 kDa, 16 µg/mL of alamethicin corresponds to ~8 µM. This is three times larger than the critical micelle concentration of alamethicin in water [17]. Micelle formation may affect the MIC and the timing of the specific mechanistic events described below.

2.4. Microscopy Experiments

The home built, temperature-controlled flow chamber has an internal volume of 60 µL (3 mm × 31 mm × 0.75 mm); its construction was described previously [13]. Polylysine coating of the coverslip to improve adherence was avoided, because it alters *B. subtilis* growth. As before [11], the coverslip was sonicated in acetone for 30 min, then rinsed with water and dried. The fully assembled flow chamber was placed in a vacuum chamber for 1–5 min, to remove unwanted bubbles, then placed onto the heated microscope stage and allowed to equilibrate to 37°C. Cells harvested from the mid-log phase liquid culture were injected into the flow chamber, and rinsed with at least 0.8 mL of fresh medium to remove unadhered cells.

The stock solution of alamethicin in ethanol was diluted in fresh, aerated EZRDM to the desired concentration (typically 1X MIC = 16 µg/mL) and thoroughly vortexed to prevent aggregation. At that dilution ratio, the concentration of ethanol in the medium that flowed through the observation chamber is 0.3% by volume. To test for possible effects of ethanol alone, we measured the MIC of ethanol in the same conditions. The 6-hr MIC is 0.9% by

volume. We also measured cell length vs time for plated cells with EZRDM and 0.3% ethanol flowing (no alamethicin). As shown in Fig. S1, cells continue growing in 0.3% ethanol but at a somewhat slower rate. The length vs time behavior using 0.3% ethanol is completely different from that using 0.3% ethanol plus 16 $\mu\text{g/mL}$, as described below.

A picture of the flow chamber is provided in Fig. S2. Alamethicin in aerated medium flows throughout the microscopy experiment, driven by syringe pumps (SyringePump, model NE-300). The bulk concentration of alamethicin is thus well defined and constant. Most experiments were performed as follows. After the cells were injected into the flow chamber and rinsed with medium, the chamber was attached to two syringe pumps through tubing connected by a y-junction. *s*-EZRDM flowed at a rate of 0.1 mL/min for the first 7 min of data acquisition, at which point the flow was switched to a second syringe containing alamethicin and 2 nM of Sytox Orange, also in *s*-EZRDM. Sytox Orange is a “dead-cell stain” with maximum absorption and emission at $\lambda_{\text{abs}} = 547$ nm and $\lambda_{\text{em}} = 570$ nm, respectively. It fluoresces strongly only on binding to DNA. Sytox Orange allows us to carry out two-color imaging of cytoplasmic GFP and DNA staining in the same cell. The initial injection of alamethicin/Sytox Orange in *s*-EZRDM was performed at 2 mL/min for 30 s in order to rapidly exchange solution conditions. The flow was then changed to 0.1 mL/min for the rest of the data acquisition to minimize consumption of alamethicin. The average doubling time for the plated GFP strain in the first 7 min period was 44 ± 5 min (\pm one standard deviation for 19 cells), based on tip-to-tip measurements of cell length vs time in phase contrast images.

The constant flow setup should maintain the bulk concentration of alamethicin in the chamber at that of the bulk solution. As a consequence, we observe major symptoms of antimicrobial stress at 1X the MIC in less than one hour after injection. In contrast, our earlier study of LL-37 used static conditions; the antimicrobial did not flow after the initial exchange of solutions. Concentrations of 2–4X the MIC were required to observe symptoms on the 1-hr observation timescale [11]. When we repeat the LL-37 experiments using the constant flow setup, the same major symptoms of antimicrobial stress appear at lower concentrations (1–2X the 6-hr MIC). In the static conditions, we believe adherence of the peptide to components of the chamber significantly reduced the bulk concentration.

Microscopy movies were obtained using a Nikon Eclipse TE300 microscope, equipped with a Nikon Phase Contrast Type DLL Objective, with NA = 1.3. All filters were from Chroma Technology. A 500 nm long-pass filter (HQ500LP) was used as the dichroic. Three different channels were imaged: cytoplasmic GFP (excitation at 488 nm from an Ar+ laser, emission filter ET525/50), Sytox Orange (excitation at 561 nm from a Coherent Sapphire laser, emission filter HQ600/50), and phase contrast (using the HQ600/50M filter). Images were captured by an Andor Ixon 897 EMCCD camera.

One-hour time lapse movies were obtained by cycling the three observation channels. GFP, Sytox Orange, and phase contrast images were taken at 6-s intervals with 50 ms exposure times each (complete cycle time 18 s). This cycle was repeated 300 times to obtain a 1-hr long movie. Growth medium alone flowed during the first 7 min, after which the flow was switched to growth medium containing alamethicin and Sytox Orange. In other experiments,

the time evolution of Sytox Orange staining of DNA was obtained as a fast, single-channel movie with 0.5-s cycle time.

2.5. Data Analysis

Movies from time-lapse imaging were analyzed using imageJ [18], and the program *microbeTracker* [19], using algorithm 4 with modifications to the following parameters: $\text{areaMin} = 300$, $\text{thresFactorM} = 1.2$, $\text{thresFactorF} = 1.2$, $\text{splitThreshold} = 2$, $\text{joindist} = 8$, $\text{joinangle} = 1.2$. Cells were selected for full analysis based on how well they remained plated and stayed in focus during the movie, as well as good separation from other cells on the plate. *MicrobeTracker* estimates the tip-to-tip cell length, as well as the cell volume, assuming that the cell is cylindrically symmetric around its long axis. Cell length precision is ~ 50 nm, as estimated from the noise in plots of length vs time. The method is described in detail in Ref. [20].

3. Results

3.1. Single Cell Attacked by Alamethicin at 1X MIC

Eighteen of the 19 *B. subtilis* cells that were fully analyzed using cytoplasmic GFP and Sytox Orange are “double cells”. These comprise two nascent daughter cells that have formed a septum and thus have two separate cytoplasmic regions (as shown below), but are still connected by their peptidoglycan layers. The septal region for *B. subtilis* is narrow (< 300 nm, [21]), and is not readily visualized by phase contrast microscopy until the cells have separated more completely. The preponderance of double cells in the sample selected for detailed study over 60 min may arise from better adherence of double cells to the glass coverslip.

We first describe and interpret the observed effects of $16 \mu\text{g/mL}$ (1X MIC) of alamethicin on the one example of a single, well isolated *B. subtilis* cell expressing cytoplasmic GFP. This single cell helps guide our interpretation of the data for double cells. Growth medium containing alamethicin and Sytox Orange was injected at $t = 0$ (Movie S1). In Fig. 1A, cell length plateaus abruptly, beginning 2–3 min after injection of alamethicin, suggesting the halting of growth. At $t = 10$ min, the cell begins to shrink in length, eventually losing $\sim 15\%$ of its length. There is gradual shrinkage at first, but most of the decrease in length occurs abruptly at $t = 11.3$ min (in < 18 s, one camera cycle). We call this an abrupt shrinkage event. Cell length subsequently remains stable. Staining of the nucleoid with Sytox Orange begins within one frame (18 s) of the abrupt shrinkage event; there is no evidence of staining at earlier times.

After addition of alamethicin at $t = 0$, the integrated GFP intensity decreases in two gradual phases for the single cell in Fig. 1. (The upward baseline drift prior to $t = 0$ is atypical, as described in detail below; it is likely due to drift in microscope focus or movement of the cell during imaging.) The first phase of GFP intensity loss shows a decrease by about 20% over the course of 6 min, beginning at $t = 5.3$ min and ending with the abrupt shrinkage event at $t = 11.3$ min. This initial decrease cannot be due to leakage of GFP out of the cell. If GFP could leak out, the much smaller molecule Sytox Orange could enter the cytoplasm, but

we do not yet observe any staining of the DNA. Instead, we suggest that alamethicin is causing gradual pH equilibration between the cytoplasm (pH ~ 7.8–8.1) and the buffered growth medium (pH = 7.4) [22, 23]. This inference is supported by a positive control using the ionophore nigericin, described below. Lower pH is known to decrease the fluorescence yield of GFP due to partial protonation of the fluorophore [15]. The rate of the initial decrease in GFP intensity is evidently limited by the rate of pH change, not by the rate of protonation of the GFP chemical state. In the earlier LL-37 study, we saw an analogous pH event using the same GFPmut3, but the change occurred much faster, on a timescale of 0.5 s or less [11]. The protonation step for GFPmut3 likely occurs on a sub-ms timescale [15, 24].

The initial decrease in GFP intensity ends in a plateau at the same time that the cell becomes permeabilized to Sytox Orange ($t = 12.0$ min). The cell envelope is retaining GFP while admitting the much smaller Sytox Orange. After a delay of about five min, there is a second phase of GFP intensity loss, which also takes about 6 min. The second decay begins at $t = 17.6$ min and ends at 23.3 min, by which time the integrated intensity is essentially zero (complete loss of GFP). We believe this is real loss of GFP from the cell envelope due to permeabilization of the membrane/peptidoglycan layer to proteins as large as GFP. The underlying cause of the lag time between Sytox Orange entry and GFP release is further investigated below.

To support the inference that the initial decrease in GFP intensity is due to a decrease in intracellular pH, we used nigericin treatment as a positive control. Nigericin is a K^+/H^+ antiporter known to quickly degrade the pH across cellular membranes by exchanging internal K^+ ions for external H^+ ions [25]. If our interpretation of the GFP signal is correct, then cells treated first with nigericin and then, after a time delay, with alamethicin should exhibit the initial decrease in GFP intensity *before* injection of alamethicin.

Figure 2A shows the GFP integrated intensity vs time for 19 individual cells treated with alamethicin alone at 16 $\mu\text{g}/\text{mL}$. The average of these intensities is shown as a thick black line. To partially correct for cell-to-cell variability in the timing of events, the data in Fig. 2A have a different time axis than the data in Fig. 1. The new time variable t' is defined with $t' = 0$ the time at which the abrupt cell shrinkage events have concluded. Thus the initial phase of GFP intensity loss occurs at $t' < 0$. Note that on average, the baseline GFP fluorescence intensity is initially flat. This corroborates the earlier assertion that in Fig. 1 the rising GFP intensity between $t = -7.5$ to $t = 5$ min is artifactual, perhaps due to drift of the microscope focus or movement of the cell during imaging, and does not reflect a real change in GFP intensity. The ~20% decrease in mean GFP intensity that begins at $t' = -5$ min occurs in all cells and is a real decrease in GFP intensity.

Figure 2B shows the effect of injection of 5 μM nigericin into the flow chamber 6 min prior to injection of alamethicin at the usual 16 $\mu\text{g}/\text{mL}$. The time axis again sets $t = 0$ as the time of alamethicin injection, as in Fig. 1. The bold line is the mean behavior of the 11 individual cells shown. Injection of nigericin at $t = -6$ min causes a prompt and abrupt decrease in GFP intensity by ~30%. Subsequent addition of 16 $\mu\text{g}/\text{mL}$ alamethicin at $t = 0$ causes no additional change in average GFP intensity over the subsequent 20 min. As before, all 11 cells exhibited an abrupt shrinkage event and the onset of Sytox Orange staining sometime

in the range $t = 0$ –14 min after alamethicin injection (data not shown). In addition, there was a sharp decrease in the slope of cell length vs time within 1 min of nigericin addition (*i.e.*, before alamethicin addition). Evidently the nigericin-induced decrease in the pmf causes an abrupt attenuation of growth. In a separate control, injection of nigericin alone causes the same abrupt decrease in GFP intensity, but cells do not shrink and Sytox Orange never enters the cytoplasm on the 50 min timescale of the observations. These data qualitatively support the inference that the initial, slow decrease in GFP intensity on treatment with alamethicin alone is caused by *gradual* degradation of the pH gradient across the cytoplasmic membrane.

3.2. Double Cells Attacked by Alamethicin at 1X MIC

The inferences from the single *B. subtilis* cell of Fig. 1 help inform our interpretation of the more complex sequence of events observed for double cells, the vast majority. A typical example is shown in Fig. 3 (and Movie S2). Phase contrast and Microbe Tracker only measure the combined double-cell length. The double-cell length decelerates almost immediately after injection of alamethicin and plateaus within 3 min, again noticeably earlier than the onset of the first decrease in GFP intensity. This is shown in detail in Sec. 3.3 below. For the double cell in Fig. 3, GFP intensity then gradually decreases by about 25% over some 5 min, from $t = 5$ min to $t = 10$ min. This behavior is similar to that observed for the single cell (Fig. 1). Based on the nigericin study (Fig. 2), we interpret the initial decrease in GFP intensity as arising from pH equilibration across the cytoplasmic membrane.

Subsequently, there are *two* abrupt cell shrinkage events, beginning at $t = 9.2$ and 11.3 min. Double-cell length plateaus for 4 frames (72 s) in between. Careful scrutiny of the phase contrast images shows that the two events correspond to shrinkage of first the right-hand cell and then the left-hand cell. This is our evidence for double cells, cells with a septum separating two cytoplasms. If the two cytoplasms were still connected, we would expect cell shrinkage to occur simultaneously in both halves. Accordingly, Sytox Orange stains the cell on the right first, and then the cell on the left. Evidence of a septal region can be seen as early as $t = 10$ min, and the septum is clearly seen by $t = 30$ min. For the 19 cells studied in detail, the average time between injection of alamethicin and completion of all cell shrinkage events is 10.9 ± 2.3 min (\pm one standard deviation).

A second, more gradual decrease in GFP intensity becomes evident as a break in slope that immediately follows the abrupt shrinkage events and the entry of Sytox Orange into the cytoplasm. We believe this is actual leakage of GFP out of the cell envelope. The intensity decrease is not primarily due to photobleaching. As shown in the earliest part of Fig. 2A, under our imaging conditions GFP shows no appreciable photobleaching over a period of at least 15 min. The second intensity decrease is occurring simultaneously in both cells, as determined by measuring the integrated intensities of the individual halves of the images as a function of time. For the double cell in Fig. 3, gradual loss of GFP intensity continues over 35 min until $t = 46.4$ min, when the left-hand cell abruptly loses all of its remaining GFP. The right-hand cell never loses all of its GFP on the 1-hr time scale of the experiment. Approximately 60% of the 19 cells studied showed this gradual decrease in GFP intensity

after cell shrinkage but before abrupt and complete loss of GFP. The remaining 40% showed no loss of GFP prior to the abrupt loss.

For the double cell of Fig. 3, after abrupt shrinkage is complete the double-cell length slowly recovers about half of its initial loss. All 18 analyzed double cells exhibited gradual increases in cell length after the abrupt shrinkage events. As argued in our previous study on LL-37, we do not believe that this is actual cell growth in the sense of production of more cellular mass. Instead, compensating changes in cell length and width preserve cell volume. In all 18 cells, cell volume (as estimated by MicrobeTracker) did not increase after shrinkage. Examples are given in Fig. S3. We utilize cell length instead of cell volume in our analysis because it is less sensitive to de-focusing of the microscope.

3.3. Growth Evidently Halts Minutes Before the Initial Decrease in GFP Intensity

Taken as a whole, the data provide strong evidence that cell growth halts before the cytoplasmic membrane becomes permeabilized to protons (detected as a decrease in GFP fluorescence intensity). However, in Figs. 1 and 3 the drifting baseline GFP intensity prior to addition of alamethicin at $t = 0$ makes it uncertain that the initial decrease in GFP intensity after $t = 0$ is real. The examples in Figs. 1 and 3 were chosen to best illustrate other features. A better example of a double cell with a flat baseline and good signal-to-noise ratio in both GFP intensity vs time and cell length vs time is shown in Fig. 4. Two other examples, including one less clear case, are shown in Fig. S4.

We estimate the lag time t between the halting of cell growth and the onset of GFP intensity decrease as follows. We draw straight lines through regions of fairly constant slope before and after the transition and take their intersection as the time of the onset of each event (Fig. 4). This helps correct for sloping baselines and gradual, rather than abrupt, changes in slope. In Fig. 4, this construction yields a lag time of $t = 2.7$ min. For the 19 cells analyzed in detail, the mean lag time was $\langle t \rangle = (2.4 \pm 1.0)$ min (\pm one standard deviation). Individual values of t ranged from 0.8 to 4.1 min. In many cases, plots of either length vs time or GFP intensity vs time curve gradually rather than making an abrupt change of slope; examples are given in Fig. S4. In those cases, our estimate of t can be uncertain by 1–2 min. However, we judge that in 17 of 19 analyzed cases, length vs time has flattened significantly before GFP intensity turns downward. In the remaining two cases, the two events could be happening simultaneously. In no case does GFP intensity clearly turn downward before length flattens.

3.4. What is the Barrier to GFP Release?

Cytoplasmic GFP is retained within the cell envelope long after the much smaller Sytox Orange penetrates the envelope and accesses the cytoplasm. We consider two possible explanations. First, alamethicin may initially permeabilize the CM to small species but not to globular proteins, as befits a barrel-stave pore. Alternatively, GFP may be able to penetrate the cytoplasmic membrane readily and early on, but it may penetrate the peptidoglycan layer only very slowly. The passageways through the thick peptidoglycan layer of *B. subtilis* presumably narrow significantly after cell shrinkage. In this view, GFP loss is initially greatly impeded by the shrunken peptidoglycan layer. The delayed, abrupt,

total loss of GFP occurring much later might then arise from the action of autolysins. These are enzymes that degrade peptidoglycan crosslinks to enable insertion of new glycan strands and cell separation [26, 27].

After cell shrinkage and permeabilization of the CM to Sytox Orange, there should be no more synthesis of peptidoglycan components due to the loss of the proton motive force and intracellular ATP. However, the autolysins, which do not require ATP, should continue to enzymatically degrade the peptidoglycan layer [28]. If this autolysin hypothesis is correct, then any agent that increases the rate of peptidoglycan degradation should decrease the time delay between length shrinkage and the abrupt GFP leakage events. To test the hypothesis, we carried out the same alamethicin experiment as before, but switched the flow from alamethicin to lysozyme plus alamethicin after all cells had undergone the abrupt shrinkage/Sytox Orange staining event. Lysozyme hydrolyzes the bond between the two sugars in the saccharide chain, N-acetylmuramic acid and N-acetylglucosamine. The question is whether or not lysozyme working in concert with the autolysins can diminish the lag time to GFP loss.

B. subtilis cells were plated in the flow chamber and imaged without alamethicin for the first 2 min of data acquisition. At $t = 0$, growth medium containing 16 $\mu\text{g}/\text{mL}$ alamethicin plus 2 nM Sytox Orange was injected at a rate of 2 mL/min for 1 min (from Syringe B, Fig. S2) to ensure prompt mixing. The flow was then changed to 0.1 mL/min. At $t = 5$ min, after all the cells had shrunk but before abrupt GFP release, the flow was changed to growth medium containing 0.2 $\mu\text{g}/\text{mL}$ lysozyme, 16 $\mu\text{g}/\text{mL}$ alamethicin, and 2 nM Sytox Orange at a rate of 2 mL/min for 30 sec (from Syringe A, Fig. S2). The flow was then changed to 0.1 mL/min for the remainder of the 60-min movie. In control experiments, flow conditions were the same, but lysozyme was omitted from the solution in Syringe A.

We define the time lag between cell shrinkage and abrupt and complete loss of GFP as $\delta t = t_{GFP} - t_{shrink}$. Here t_{shrink} is the time of cell shrinkage, and t_{GFP} is the time at which each cell fully loses its GFP. For example, for the cell in Fig. 1, $\delta t = 23.3 \text{ min} - 11.6 \text{ min} = 11.7 \text{ min}$. For the double cell in Fig. 3, the event for the left cell would be recorded as $\delta t = 48.8 \text{ min} - 11.3 \text{ min} = 37.5 \text{ min}$. The cell on the right does not undergo an abrupt GFP loss, and would not be included in our analysis. When abrupt loss from both cells in a double cell was observed, both events were counted and two δt values were recorded. We use the end of GFP leakage and not the beginning because it provides a more precise timing measure.

The distribution of δt values for cells exposed to lysozyme after addition of alamethicin is compared with that of the alamethicin-only experiments in Fig. 5. A total of 36 cells were measured for these experiments. The distributions overlap, but there is a significant shift in the mean of the distribution of δt values to shorter times when cells are exposed to lysozyme after shrinkage. The mean value $\langle \delta t \rangle$ shifts from $(34 \pm 11) \text{ min}$ to $(20 \pm 5) \text{ min}$ when lysozyme is included. In an additional control, we applied the same 0.2 $\mu\text{g}/\text{mL}$ of lysozyme alone to *B. subtilis* cells. This causes neither loss of GFP nor cell shrinkage on a one hour timescale (data not shown).

Evidently interaction of lysozyme plus autolysins with the peptidoglycan layer after alamethicin has permeabilized the membrane to Sytox Orange shortens the mean time to GFP loss as compared with autolysins alone. These data support the hypothesis that the peptidoglycan layer forms the primary barrier to GFP efflux. If so, then the time at which the cytoplasmic membrane becomes permeabilized to GFP cannot be determined by these methods.

3.5. Abrupt, Delocalized Staining of the *B. subtilis* Nucleoids by Sytox Orange

In our study of LL-37 action on *B. subtilis*, single-channel movies with 2-s time resolution revealed that Sytox Green initially stained only a small, punctal region of the nucleoids. The staining then spread across the entire nucleoid volume over the subsequent ~1–2 min. This indicated initially localized membrane disruption; Sytox Green was able to enter the cytoplasm only at a specific location within the membrane.

To enable appropriate comparisons, we have measured single-channel, Sytox Orange movies with 0.5-s time resolution for both alamethicin and LL-37, flowing the AMP in both cases. Representative examples of the nucleoid staining dynamics of *B. subtilis* cells exposed to 2 μM LL-37 or 16 $\mu\text{g}/\text{mL}$ alamethicin (2X and 1X the MIC, respectively) are compared in Fig. 6 (and Movies S3 and S4). Due to the lag time between injection and cell shrinkage and the fast imaging rate, injection of the AMP occurred prior to the start of the movie. The exact time of cell shrinkage is unknown, but it probably occurs within 30 s of the onset of Sytox Orange fluorescence.

As before, cells exposed to LL-37 display initially localized Sytox Orange staining that spreads to the entire nucleoid on a ~1 min timescale. In contrast, alamethicin causes essentially uniform staining of the nucleoid in the earliest frames exhibiting appreciable signal-to-noise ratio, *i.e.*, within ~5 s of the onset of visible staining. The LL-37 data indicate that diffusion of Sytox Orange from a localized source across the nucleoid takes 30–40 s at a minimum, presumably due to strong binding of the dye to DNA. This strongly suggests that diffusion is too slow to explain the uniform staining induced by alamethicin on the 5-s timescale. Within the spatial resolution of the microscopy experiments, alamethicin permeabilizes the entire membrane to Sytox Orange in a delocalized fashion within ~5 s. We call this “global permeabilization”, in contrast with the “localized permeabilization” induced by LL-37.

3.6. Long Term Effects of Exposure to Alamethicin

We attempted to observe the effects of alamethicin on *B. subtilis* at longer time scales. Unfortunately, cells that have shrunk due to alamethicin action tend to detach from the coverslip, severely limiting our ability to observe many cells for longer time periods. Some cells remain adherent for several hours. These typically lose phase contrast on a time scale of 2–4 hr. An example is shown in Fig. S5. Complete loss of phase contrast indicates permeabilization of the cell envelope to the chromosomal DNA, ribosomes, and other large cytoplasmic species. The “ghost-like” remaining images indicate that a remnant of the cell envelope remains, *i.e.*, the entire envelope is not solubilized. Similar events were observed at long times in our earlier study of LL-37 on *B. subtilis* [11].

4. Discussion

The MIC of alamethicin is threefold higher than its critical micelle concentration in water [17]. The species impinging on the *B. subtilis* cells is likely micelles comprising some 16 alamethicin molecules each. This is somewhat analogous to the situation in the earlier study of the attack of LL-37 on *B. subtilis* [11]. LL-37 is known to fold to amphipathic helices and form bundles in salty solution. It is difficult to assess the degree to which micellization of alamethicin or bundling of LL-37 affect the timing of the mechanisms observed by our assays.

The data strongly suggest that alamethicin causes the halting of *B. subtilis* growth several minutes *before* permeabilization of the membrane to protons. The evidence comes from the observation that the break in slope of cell length vs time occurs on average $\langle t \rangle = (2.4 \pm 1.0)$ min before the onset of the gradual decrease in GFP intensity (average over 19 cells; example in Fig. 4). The data unambiguously demonstrate that growth halts before permeabilization of the cytoplasmic membrane to the dye molecule Sytox Orange (Figs. 1 and 3). In our earlier single-cell study of LL-37 on *B. subtilis*, at concentrations too low to induce CM permeabilization and cell shrinkage, we observed a possibly analogous deceleration of growth without membrane permeabilization [11].

While we interpret the gradual, delayed decrease in GFP intensity as arising from gradual acidification of the cytoplasm (Fig. 4), we do not fully understand the magnitude of the change. The fractional decrease in GFPmut3 fluorescence intensity induced by alamethicin is ~20% on average (Fig. 2A); that induced by the nigericin control is even larger, ~30% on average (Fig. 2B). Both responses are significantly larger than those found earlier for the same GFPmut3 as the pH decreased from 8.0 to 7.4, the relevant range here. In a study of cytoplasmic GFPmut3 in *B. subtilis* cells suspended in buffer of known pH containing nigericin (to equilibrate pH across the CM), fluorescence from cytoplasmic GFPmut3 decreased by 10–13% as pH changed from 8.0 to 7.4 [29]. In sensible agreement, the fluorescence intensity of purified GFPmut3 in buffer decreased by 13% as the pH decreased from 8.0 to 7.4 [16].

If the halting of growth and permeabilization of the membrane to protons were occurring simultaneously, we should have observed a significant decrease in GFP intensity earlier on, when growth halted. An average 13% decrease would be readily detectable (Fig. 2A), but we observe no such prompt decrease. It is not clear why the delayed, gradual decrease in GFP intensity caused by alamethicin (20%) and the abrupt decrease caused by nigericin (30%) are significantly larger.

Additional mechanisms may be at work. Two possibilities are the induction of oxidative stress due to interference with the electron transport chain and interference with cell wall assembly, both of which could be induced with the cytoplasmic membrane intact. There is a hint from earlier work that oxidative stress may decrease GFP intensity. We studied the attack of the synthetic peptide CM15 on *E. coli* cells expressing GFPmut3 that was exported to the periplasm by the Tat system [9]. Essentially simultaneously with *E. coli* cell shrinkage and cytoplasmic membrane permeabilization, two intra-cellular reporters of oxidative stress

showed enhanced fluorescence. At the same time, periplasmic GFP moved inward (into the cytoplasm) and exhibited a 15% *decrease* in intensity. Equilibration of pH across the membrane and transfer of GFP to the cytoplasm should cause no change in GFP intensity if the cytoplasm, periplasm, and surround all reach the same pH. Instead, intensity decreased, indicating some other mechanism. It might be informative to apply the same single-cell oxidative stress reporters to the attack of alamethicin on *B. subtilis*.

If our interpretation of the GFP intensity decrease as primarily due to the change in pH is essentially correct, then loss of the pmf due to alamethicin is gradual, typically occurring over some five minutes. During this loss, cell length remains constant and Sytox Orange is not yet able to penetrate the OM. Gradual loss of the pmf might arise from the formation of small, transient membrane disruptions. The stability of cell length and volume during this phase of membrane disruption argues against formation of barrel stave pores like those observed by Huang and co-workers in lipid multilayers at high P/L ratios. Neutron scattering found pore diameters varying from 1.8 nm (~8 α -helices) to ~2.6 nm (~11 α -helices), depending on the lipid used [4]. A 1.8 nm pore would pass numerous small ionic and neutral osmolytes, causing cell shrinkage, but this does not yet occur.

The abrupt onset of permeabilization of the CM to Sytox Orange occurs concomitantly with abrupt shrinkage of cell length by about 15%. The hydrodynamic radius of Sytox Orange (1 kDa) is ~1 nm, assuming it is similar to that of Sytox Green [30]. We attribute cell shrinkage to loss of small osmolytes from the cytoplasm. Once the CM is permeabilized to Sytox Orange, it should leak small ions, ATP, and other small species. The turgor pressure should decrease at the same time the cell shrinks in length, although turgor is not measured directly. We made similar observations for LL-37 at sufficiently high concentration [11].

Alamethicin induces *global* permeabilization of the CM to Sytox Orange. The entire periphery of the cell begins to admit Sytox Orange within a period of at most 5 s (Fig. 6). This global permeabilization behavior contrasts sharply with the behavior of LL-37, which induces *localized* permeabilization of the CM to Sytox Orange. Due to the limited spatial resolution of light microscopy, apparently global permeabilization could arise from the nearly simultaneous formation of *many* local disruptions. Perhaps as the alamethicin concentration at the CM builds up, the smaller transient membrane disruptions that enabled proton equilibration across the CM nucleate to form widely distributed pores sufficiently large to pass Sytox Orange. Alternatively, the data are also consistent with a “global carpet” mechanism in which the membrane is abruptly “solubilized” by the amphipathic AMP once the concentration has built up sufficiently.

After Sytox Orange entry and cell shrinkage, GFP gradually leaks out of the cell envelope over tens of minutes, followed by more abrupt loss of all remaining GFP, usually some 5–40 min later. Some cells never completely lose GFP over 60 min. Evidently the shrunken cell envelope has become mildly permeable to GFP. The structure of GFP is an 11-stranded β -barrel of diameter ~3 nm and height ~4 nm [31]. GFP presumably cannot transit an 8-helix, 1.8 nm diameter alamethicin barrel stave pore; it might slowly transit an 11-helix, 2.6 nm diameter pore. It is also possible that after the cell shrinkage event, the peptidoglycan layer is typically limiting the rate of efflux of the 27 kDa GFP. The porosity of the normal

peptidoglycan layer in *B. subtilis* (as stretched by the turgor pressure) has an estimated maximum mass cutoff of ~50 kDa [32]. The relaxed layer after shrinkage may impede GFP passage, but allow slow passage. In the Gram negative *E. coli*, the peptidoglycan layer evidently does not form an effective diffusion barrier against periplasmic GFP [12, 13]. This is consistent with the much thinner layer in *E. coli* [33].

Eventually, at a widely variable time in the range ~5–40 min or longer, the cell envelope abruptly springs a larger leak to GFP, which is then completely lost to the cell over a period of several minutes (Figs. 1 and 3). The experiments in which we inject first alamethicin and then change the flow to lysozyme plus alamethicin 5 min later show that lysozyme hastens the onset of this larger leak (Fig. 5). This suggests the larger leak may arise from abrupt formation of a large breach in the peptidoglycan layer. We therefore suggest that absent lysozyme, the autolysins cause a similar disruption, but on a longer timescale. If this is correct, then the abrupt transition in the loss rate of GFP is due to a disruption of the peptidoglycan layer, not of the CM.

An emerging theme is the multi-pronged nature of the attack of antimicrobial peptides on bacterial cells [34, 35]. This may help explain their persistent efficacy over thousands of years. The strength of our single-cell methodology lies in the ability to observe a sequence of “symptoms” of antimicrobial attack in real time. In the present case of the attack of alamethicin on *B. subtilis*, the data reveal sequential permeabilization of the cell envelope first to protons, then to Sytox Orange (and by inference to small osmolytes and ATP), and finally to GFP (and other globular proteins). Some of these steps are consistent with formation of the barrel stave pores observed *in vitro*, but they do not rule out “chaotic pore” and “carpet” mechanisms. Importantly, the initial halting of growth evidently precedes these membrane-damaging events, in contrast to the widely held belief that pore formation is the usual underlying cause of bacteriostatic effects. In Gram positive species, the peptidoglycan layer and the enzymes that synthesize it are immediately exposed to AMPs. In contrast, in Gram negative species the rate-limiting step in the halting of growth seems to be translocation across the outer membrane layer [9, 12, 13].

Supplementary Material

Refer to Web version on PubMed Central for supplementary material.

Acknowledgments

Research reported in this publication was supported by the National Institute of General Medical Sciences of the National Institutes of Health under Award Number R01GM094510 (to JCW as PI) and R01GM093265 (to JCW and SHG as co-PIs). The content is solely the responsibility of the authors and does not necessarily represent the official views of the National Institutes of Health.

Abbreviations

AMP	antimicrobial peptide
pmf	proton motive force

MIC	minimum inhibitory concentration
P/L	peptide to lipid ratio
s-EZRDM	EZ rich, defined medium optimized for growth of <i>B. subtilis</i>

References

1. Leitgeb B, Szekeres A, Manczinger L, Vagvolgyi C, Kredics L. The history of alamethicin: a review of the most extensively studied peptaibol. *Chem Biodivers.* 2007; 4:1027–1051. [PubMed: 17589875]
2. Kredics L, Szekeres A, Czifra D, Vagvolgyi C, Leitgeb B. Recent results in alamethicin research. *Chem Biodivers.* 2013; 10:744–771. [PubMed: 23681724]
3. Stella L, Burattini M, Mazzuca C, Palleschi A, Venanzi M, Coin I, Peggion C, Toniolo C, Pispisa B. Alamethicin interaction with lipid membranes: a spectroscopic study on synthetic analogues. *Chem Biodivers.* 2007; 4:1299–1312. [PubMed: 17589867]
4. He K, Ludtke SJ, Worcester DL, Huang HW. Neutron scattering in the plane of membranes: structure of alamethicin pores. *Biophys J.* 1996; 70:2659–2666. [PubMed: 8744303]
5. Qian S, Wang W, Yang L, Huang HW. Structure of the alamethicin pore reconstructed by x-ray diffraction analysis. *Biophys J.* 2008; 94:3512–3522. [PubMed: 18199659]
6. Duclohier H, Wroblewski H. Voltage-dependent pore formation and antimicrobial activity by alamethicin and analogues. *J Membr Biol.* 2001; 184:1–12. [PubMed: 11687873]
7. Beven L, Helluin O, Molle G, Duclohier H, Wroblewski H. Correlation between antibacterial activity and pore sizes of two classes of voltage-dependent channel-forming peptides. *Biochim Biophys Acta.* 1999; 1421:53–63. [PubMed: 10561471]
8. Kirschbaum J, Krause C, Winzheimer RK, Bruckner H. Sequences of alamethicins F30 and F50 reconsidered and reconciled. *J Pept Sci.* 2003; 9:799–809. [PubMed: 14658799]
9. Choi H, Yang Z, Weisshaar JC. Single-cell, real-time detection of oxidative stress induced in *Escherichia coli* by the antimicrobial peptide CM15. *Proc Natl Acad Sci U S A.* 2015; 112:E303–E310. [PubMed: 25561551]
10. Bakshi S, Choi H, Rangarajan N, Barns KJ, Bratton BP, Weisshaar JC. Nonperturbative imaging of nucleoid morphology in live bacterial cells during an antimicrobial peptide attack. *Appl Environ Microbiol.* 2014; 80:4977–4986. [PubMed: 24907320]
11. Barns KJ, Weisshaar JC. Real-time attack of LL-37 on single *Bacillus subtilis* cells. *Biochim Biophys Acta.* 2013; 1828:1511–1520. [PubMed: 23454084]
12. Rangarajan N, Bakshi S, Weisshaar JC. Localized permeabilization of *E coli* membranes by the antimicrobial peptide Cecropin A. *Biochemistry.* 2013; 52:6584–6594. [PubMed: 23988088]
13. Sochacki KA, Barns KJ, Bucki R, Weisshaar JC. Real-time attack on single *Escherichia coli* cells by the human antimicrobial peptide LL-37. *Proc Natl Acad Sci U S A.* 2011; 108:E77–E81. [PubMed: 21464330]
14. Wimley WC, Hristova K. Antimicrobial peptides: successes, challenges and unanswered questions. *J Membr Biol.* 2011; 239:27–34. [PubMed: 21225255]
15. Kneen M, Farinas J, Li Y, Verkman AS. Green fluorescent protein as a noninvasive intracellular pH indicator. *Biophys J.* 1998; 74:1591–1599. [PubMed: 9512054]
16. Doherty GP, Bailey K, Lewis PJ. Stage-specific fluorescence intensity of GFP and mCherry during sporulation in *Bacillus subtilis*. *BMC Res Notes.* 2010; 3:303. [PubMed: 21073756]
17. Stankowski S, Schwarz G. Lipid dependence of peptide-membrane interactions. Bilayer affinity and aggregation of the peptide alamethicin. *FEBS Lett.* 1989; 250:556–560. [PubMed: 2753150]
18. Rasband, WS. ImageJ. Maryland, USA: B. U.S. National Institutes of Health; 1997. <http://rsb.info.nih.gov/ij/>
19. Jacobs-Wagner C. MicrobeTracker Suite. 2011

20. Bakshi S, Choi H, Mondal J, Weisshaar JC. Time-dependent effects of transcription- and translation-halting drugs on the spatial distributions of the *Escherichia coli* chromosome and ribosomes. *Mol Microbiol.* 2014; 94:871–887. [PubMed: 25250841]
21. Birdsell DC, Doyle RJ, Morgenstern M. Organization of teichoic acid in the cell wall of *Bacillus subtilis*. *J Bacteriol.* 1975; 121:726–734. [PubMed: 803488]
22. Martinez KA 2nd, Kitko RD, Mershon JP, Adcox HE, Malek KA, Berkmen MB, Slonczewski JL. Cytoplasmic pH response to acid stress in individual cells of *Escherichia coli* and *Bacillus subtilis* observed by fluorescence ratio imaging microscopy. *Appl Environ Microbiol.* 2012; 78:3706–3714. [PubMed: 22427503]
23. Breeuwer P, Drocourt J, Rombouts FM, Abee T. A Novel Method for continuous determination of the intracellular pH in bacteria with the internally conjugated fluorescent probe 5 (and 6-)-carboxyfluorescein succinimidyl ester. *Appl Environ Microbiol.* 1996; 62:178–183. [PubMed: 16535209]
24. Wilks JC, Slonczewski JL. pH of the cytoplasm and periplasm of *Escherichia coli*: rapid measurement by green fluorescent protein fluorimetry. *J Bacteriol.* 2007; 189:5601–5607. [PubMed: 17545292]
25. Margolis LB, Novikova IY, Rozovskaya IA, Skulachev VP. K⁺/H⁺-antiporter nigericin arrests DNA synthesis in Ehrlich ascites carcinoma cells. *Proc Natl Acad Sci U S A.* 1989; 86:6626–6629. [PubMed: 2771947]
26. Vollmer W, Joris B, Charlier P, Foster S. Bacterial peptidoglycan (murein) hydrolases. *FEMS Microbiol Rev.* 2008; 32:259–286. [PubMed: 18266855]
27. Smith TJ, Blackman SA, Foster SJ. Autolysins of *Bacillus subtilis*: multiple enzymes with multiple functions. *Microbiol.* 2000; 146(Pt 2):249–262.
28. Jolliffe LK, Doyle RJ, Streips UN. The energized membrane and cellular autolysis in *Bacillus subtilis*. *Cell.* 1981; 25:753–763. [PubMed: 6793239]
29. Kitko RD, Cleeton RL, Armentrout EI, Lee GE, Noguchi K, Berkmen MB, Jones BD, Slonczewski JL. Cytoplasmic acidification and the benzoate transcriptome in *Bacillus subtilis*. *PLoS One.* 2009; 4:e8255. [PubMed: 20011599]
30. Briandet R, Lacroix-Gueu P, Renault M, Lecart S, Meylheuc T, Bidnenko E, Steenkeste K, Bellon-Fontaine MN, Fontaine-Aupart MP. Fluorescence correlation spectroscopy to study diffusion and reaction of bacteriophages inside biofilms. *Appl Environ Microbiol.* 2008; 74:2135–2143. [PubMed: 18245240]
31. Yang F, Moss LG, Phillips GN Jr. The molecular structure of green fluorescent protein. *Nat Biotechnol.* 1996; 14:1246–1251. [PubMed: 9631087]
32. Demchick P, Koch AL. The permeability of the wall fabric of *Escherichia coli* and *Bacillus subtilis*. *J Bacteriol.* 1996; 178:768–773. [PubMed: 8550511]
33. Vollmer W, Blanot D, de Pedro MA. Peptidoglycan structure and architecture. *FEMS Microbiol Rev.* 2008; 32:149–167. [PubMed: 18194336]
34. Hancock RE, Sahl HG. New strategies and compounds for anti-infective treatment. *Curr Opin Microbiol.* 2013; 16:519–521. [PubMed: 23998895]
35. Wenzel M, Chiriac AI, Otto A, Zweyck D, May C, Schumacher C, Gust R, Albada HB, Penkova M, Kramer U, Erdmann R, Metzler-Nolte N, Straus SK, Bremer E, Becher D, Brotz-Oesterhelt H, Sahl HG, Bandow JE. Small cationic antimicrobial peptides delocalize peripheral membrane proteins. *Proc Natl Acad Sci U S A.* 2014; 111:E1409–E1418. [PubMed: 24706874]

Highlights

- Time-resolved imaging study of the attack of alamethicin on *B. subtilis*.
- Evidence that growth halts before permeabilization of the cytoplasmic membrane (CM).
- Permeabilization occurs uniformly across entire membrane in <5 sec, not locally.
- Shrunken cell envelope retains GFP for tens of minutes, then releases it abruptly.
- Cell envelope is permeabilized to larger and larger species as time goes on.

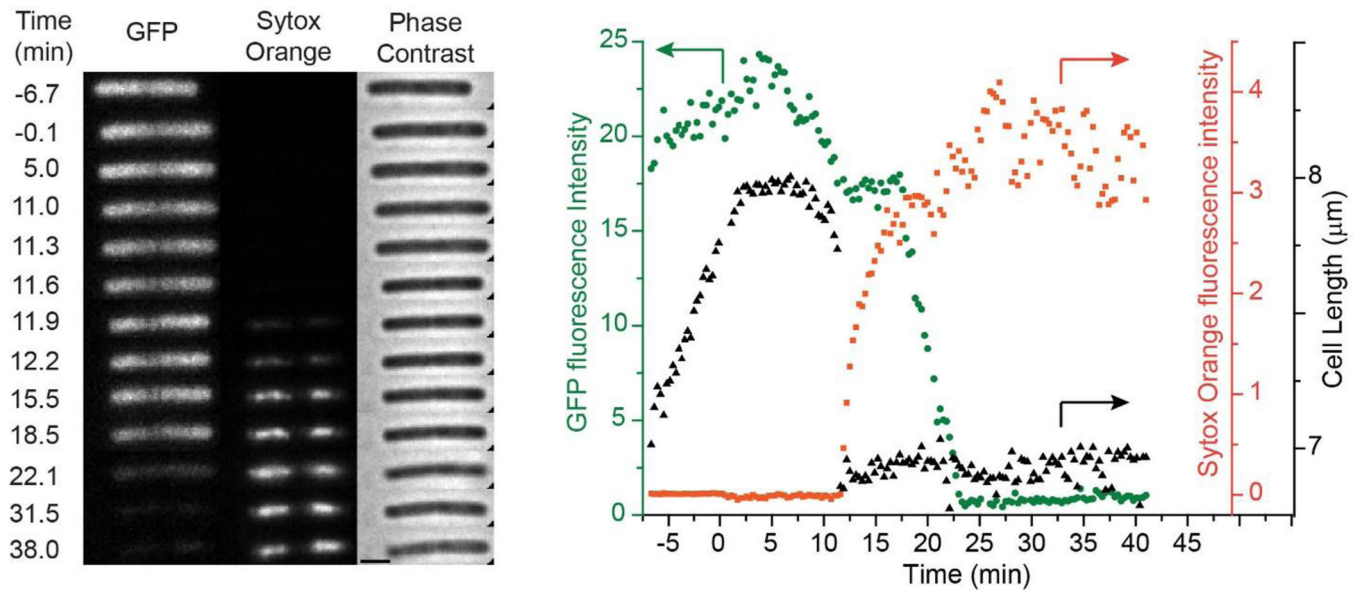


Figure 1.

Left: Three channel montage of images vs time for a single *B. subtilis* cell exposed to 16 $\mu\text{g}/\text{mL}$ alamethicin (1X MIC) and 2 nM Sytox Orange beginning at $t = 0$. Fluorescence images of cytoplasmic GFP and Sytox Orange and phase contrast images were obtained at times shown. Scale bar is 2 μm . *Right:* For the same cell, plots of total GFP intensity (green circles), total Sytox Orange intensity (orange squares), and cell length (black triangles) vs time. Arrows point to the appropriate axis for each plot. Only one single cell was amenable to quantitative analysis.

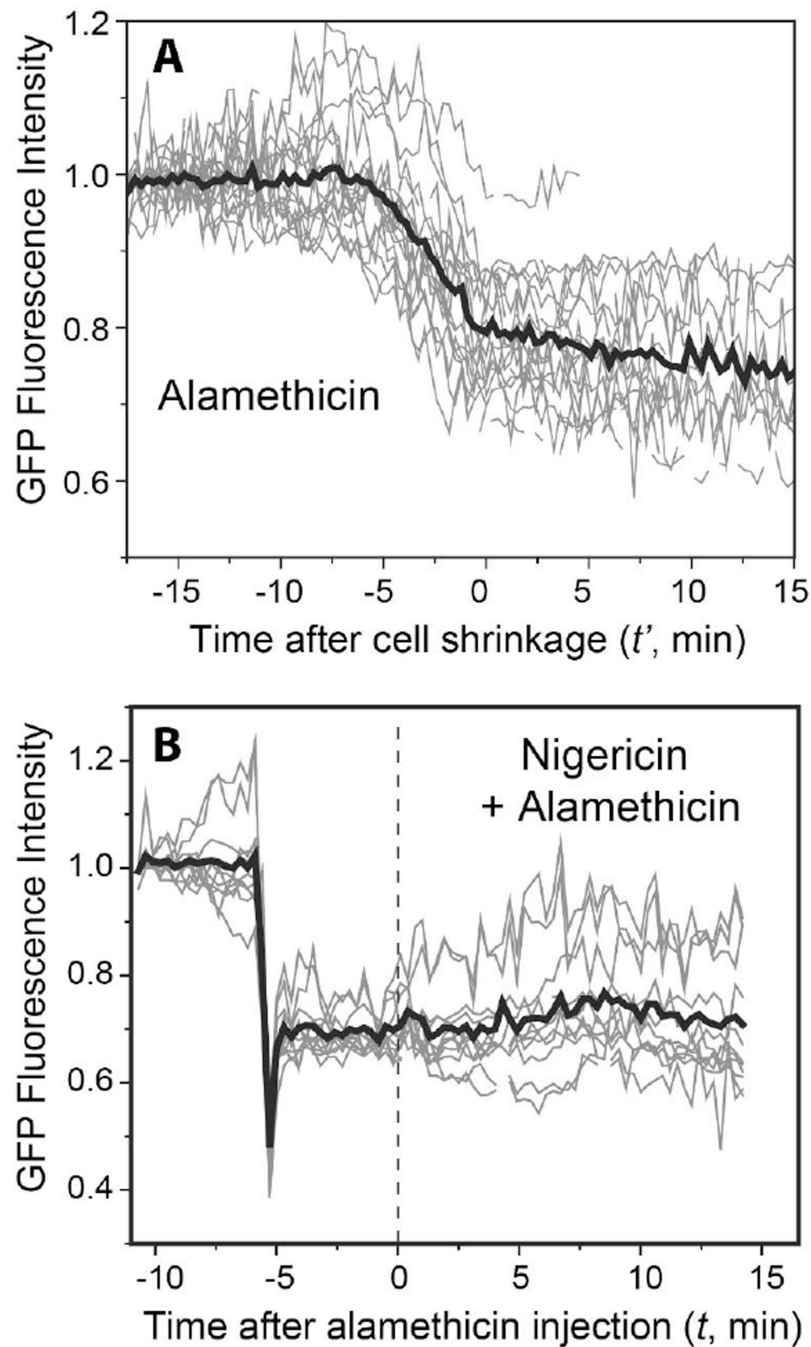


Figure 2.

(A) Normalized total GFP fluorescence intensity vs time for 19 cells exposed to 16 $\mu\text{g}/\text{mL}$ alamethicin (thin gray lines). For phasing, this plot defines time $t' = 0$ as the end of the abrupt cell shrinkage event. The average of all 19 traces is shown as the heavy black line. The time of alamethicin injection varies from $t' = -17.1$ to -7.5 min. The average decrease in GFP intensity is 20%. (B) Normalized total GFP fluorescence intensity for 11 cells treated with 5 μM nigericin at $t = -6$ min. At $t = 0$ the flow was changed to 5 μM nigericin plus 16

$\mu\text{g/mL}$ alamethicin. The average of all 11 traces is shown as the heavy black line. The nigericin-induced decrease in GFP intensity from plateau to plateau is $\sim 30\%$.

Author Manuscript

Author Manuscript

Author Manuscript

Author Manuscript

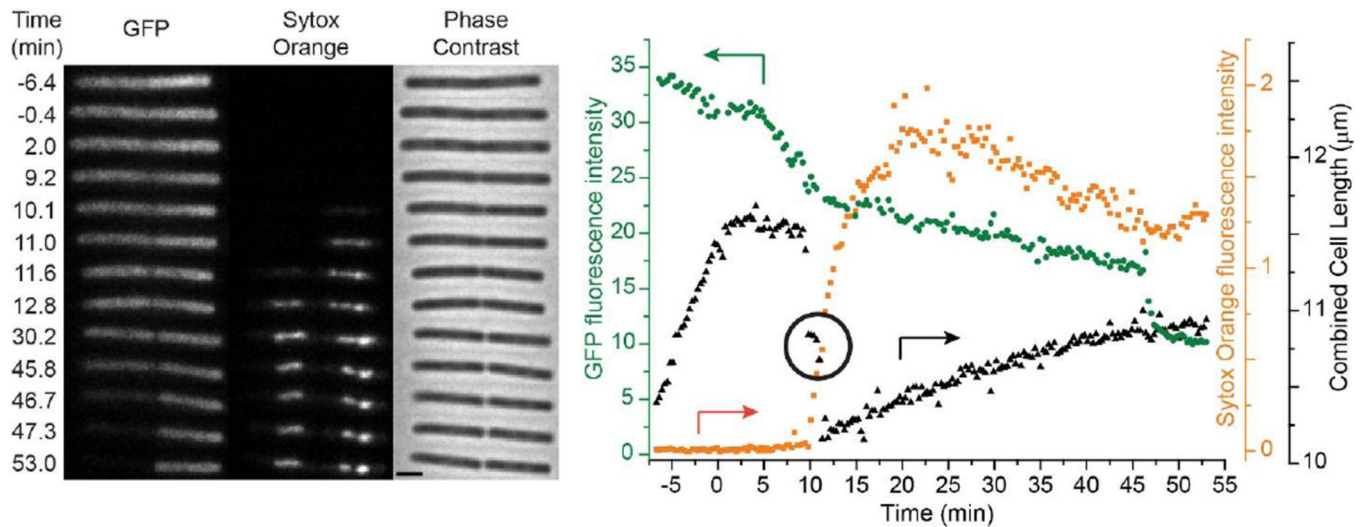


Figure 3.

Left: Three channel montage of images vs time for a representative double *B. subtilis* cell exposed to 16 μg/mL alamethicin (1X MIC) and 2 nM Sytox Orange beginning at $t = 0$. Fluorescence images of cytoplasmic GFP and Sytox Orange and phase contrast images were obtained at times shown. Scale bar is 2 μm. *Right:* For the same cell, plots of total GFP intensity (green circles), total Sytox Orange intensity (orange squares), and cell length (black triangles) vs time. Arrows point to the appropriate axis for each plot. The circled region highlights the time between the first and second abrupt cell shrinkage events. Eighteen of the 19 cells analyzed were double cells with behavior comparable to that shown here.

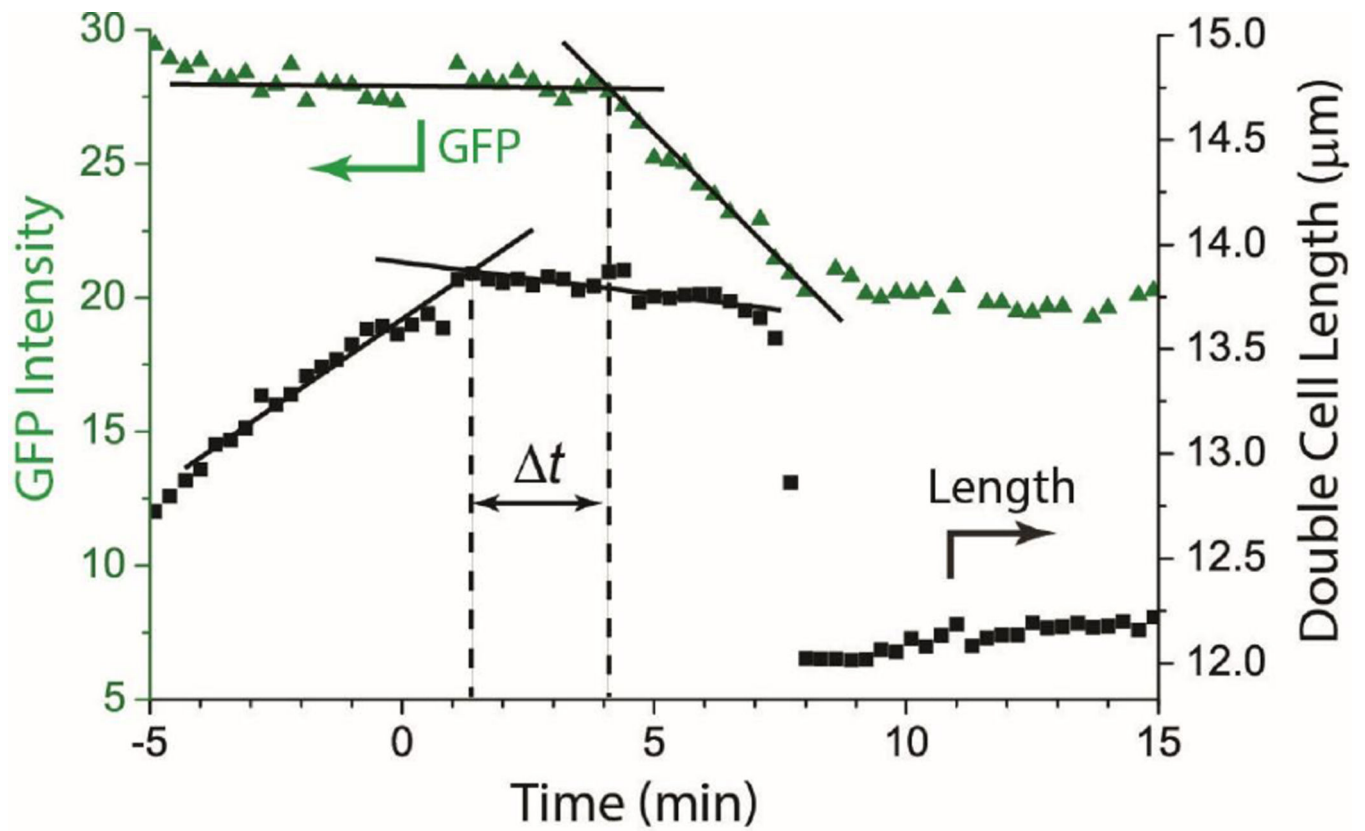


Figure 4.

Example of cell length and GFP intensity vs time plot for one double cell. Cell length flattens rather abruptly well before the GFP intensity begins to decrease. The construction shown is used to measure the lag time between the two events; $t = 2.7$ min in this case. See Fig. S4 for additional examples, one of which exhibits transitions that are less sharp in time.

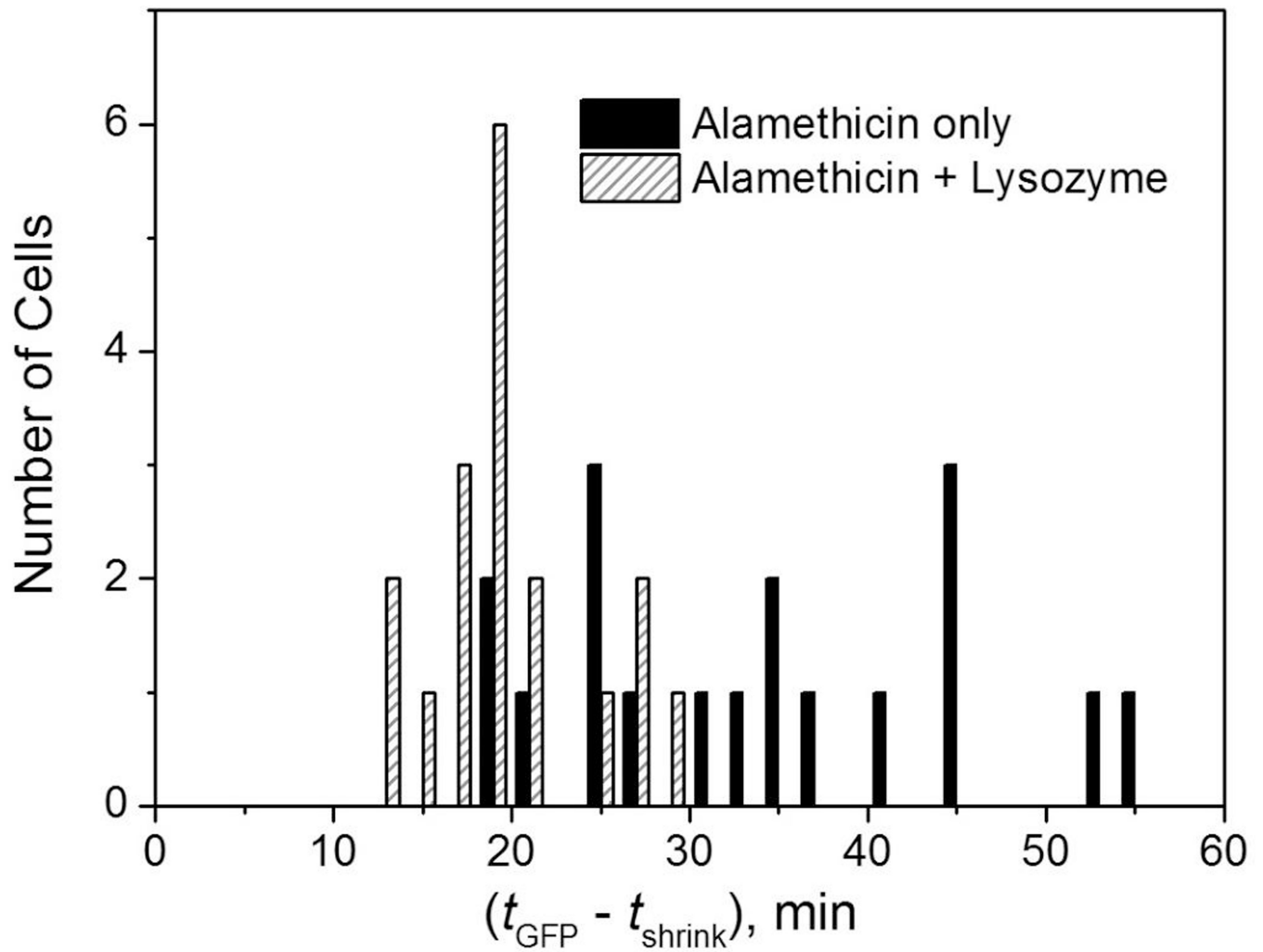


Figure 5.

Distribution of lag times between abrupt cell shrinkage and the onset of complete loss of GFP from the cell envelope. Black bars are for 18 cells exposed to 16 $\mu\text{g}/\text{mL}$ alamethicin. Cross-hatched bars are for 17 cells exposed to 16 $\mu\text{g}/\text{mL}$ alamethicin plus lysozyme at 0.2 $\mu\text{g}/\text{mL}$, with lysozyme added $t = 5$ min, after cell shrinkage had occurred. The mean value of $(t_{\text{GFP}} - t_{\text{shrink}})$ is 34 ± 11 min with alamethicin alone and 20 ± 5 min with alamethicin plus lysozyme (± 1 standard deviation).

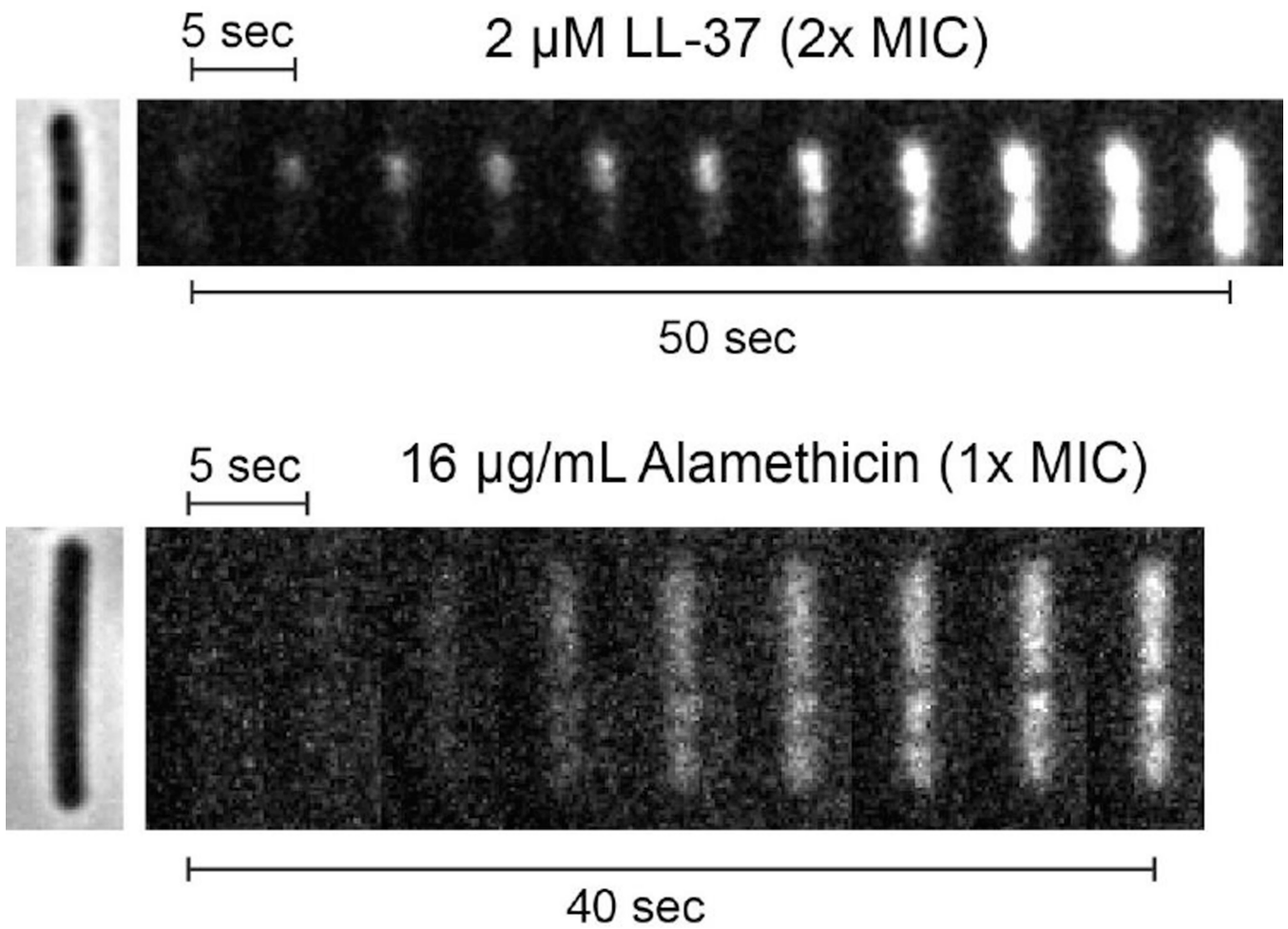


Figure 6. Comparison of dynamics of nucleoid staining by Sytox Orange exposed to 2 μ M LL-37 (*top*, 2X MIC) vs 16 μ g/mL alamethicin (*bottom*, 1X MIC). A single phase contrast image was taken before the start of the Sytox Orange data acquisition, as shown at left. Data were taken at 0.5 sec/frame; every 10th frame is shown.